

- Full paper contribution
  - August 2015
  - 7576 words in the main text, along with 5 tables and 13 figures
- 

## **Error behaviour in explicit integration algorithms with automatic substepping**

### Author 1

- Martí Lloret-Cabot, Ph.D
- ARC Centre of Excellence for Geotechnical Science and Engineering, Faculty of Engineering and Built Environment, The University of Newcastle, Australia

### Author 2

- Scott W. Sloan, Prof
- ARC Centre of Excellence for Geotechnical Science and Engineering, Faculty of Engineering and Built Environment, The University of Newcastle, Australia

### Author 3

- Daichao Sheng, Prof
- ARC Centre of Excellence for Geotechnical Science and Engineering, Faculty of Engineering and Built Environment, The University of Newcastle, Australia

### Author 4

- Andrew J. Abbo, A/Prof
- ARC Centre of Excellence for Geotechnical Science and Engineering, Faculty of Engineering and Built Environment, The University of Newcastle, Australia

### Corresponding author

Martí Lloret Cabot

[Marti.Lloretcabot@newcastle.edu.au](mailto:Marti.Lloretcabot@newcastle.edu.au)

Faculty of Engineering and Built Environment

University of Newcastle

Callaghan, Building EA

NSW 2308

Australia

Tel. +61 2 4921 5660

## ABSTRACT

This paper studies the behaviour of the error incurred when numerically integrating the elasto-plastic mechanical relationships of a constitutive model for soils using an explicit substepping formulation with automatic error control. The consistent update of all the variables involved in the numerical integration of the incremental strain-strain relationships is central to the accuracy and performance of the integration scheme and, although often missed in the literature, all variables (including specific volume and, for the case of unsaturated soils, also degree of saturation) should be explicitly considered in the algorithmic formulation. This is demonstrated in the paper by studying, in the context of the Cam clay formulations for saturated soils, the influence that the updating of the specific volume has on the accuracy of the numerical solution. The fact that the variation of the local error with the size of the integrated strain depends on the order of local accuracy of the numerical method is also used in the paper to propose a simple and powerful strategy to verify the correctness of the implemented mathematical formulation.

## INTRODUCTION

When using the finite element (FE) method with elasto-plastic constitutive models in geotechnical engineering, the *local* (i.e. within the element) integration of the incremental stress-strain relationships plays a central role because it is used repetitively within each finite element ([1-2]). During a typical iteration in a coupled FE analysis under fully saturated conditions, the nodal displacement and pore fluid pressure increments are usually found from the discretized *global* stiffness equations and these are combined with the strain-displacement relations to find the corresponding strain increments at a finite number of Gauss points within each element. The known strain and pore water pressure increments are then used at the local level to find the corresponding increments of the effective stresses (i.e. difference between total stress and pore water pressure) by integrating the mechanical constitutive model via a numerical integration scheme. In this type of formulation, the local integration algorithm is expressed in terms of the *known* strain increments and is, hence, typically referred to as a strain-driven algorithm. Various strategies have been proposed for the numerical integration of the stress-strain relations and these are typically classified as explicit algorithms (stresses are determined from the stress state at the start of the strain increment, i.e. integration at a given step/iteration progresses forward), implicit (stresses are determined from the stress state at the end of the increment, i.e. integration at a given step/iteration progresses backward with the need of an iterative scheme) or mixed formulations combining features from both schemes. The work presented here focuses on explicit formulations applied to saturated soils and, more specifically, on the family of explicit substepping algorithms with automatic error control proposed in Sloan *et al.* [3]. Discussions on the advantages and disadvantages between implicit and explicit integration schemes can be found elsewhere [3-6].

Substepping schemes with error control are particularly suited for FE applications because they control the local error in the computed variables (i.e. the effective stresses and hardening parameters) that arise due to the inexact integration of the mechanical constitutive relationships when using a numerical integration method. In this family of integration schemes the error is controlled by using a measure of the local truncation error, which is estimated as the difference between the approximate solutions from two integration schemes of different order. How much these two approximations differ from

each other is indicative of the deviation of the numerical solution from the true solution and, consequently, such a difference can be used to estimate the local truncation error. This local error estimate is then employed in the algorithm to automatically adjust the size of the integration step by reducing/increasing its current size (i.e. substepping) when the local error estimate is larger/smaller than a specified tolerance. Since the early work of Sloan [7], substepping schemes with error control have been used to integrate a large number of elasto-plastic constitutive models for saturated (e.g. [3, 8-12]) and unsaturated soil behaviour (e.g. [13-20]).

Before implementing a constitutive model into a FE code, it is advisable to verify the computational performance of the strain-driven algorithm. Such a verification process commonly compares the numerical outcomes against available analytical solutions. This task, however, is not always simple due to the scarcity of analytical solutions when employing complex constitutive relationships. Thus, a common alternative is to compare of the numerical outcomes against a *reference* solution which has been obtained using a high order substepping integration scheme with very stringent tolerances. Because in such cases the comparison is not carried out against the correct solution, it is advisable to perform a further verification and check if the local error in the numerical approximation converges with its expected order of accuracy.

Surprisingly, studies of the error incurred in the explicit substepping schemes are rarely available in the literature, even though they provide a simple complementary alternative to verify the correctness of the implemented mathematical formulation. The fact that the variation of the local error with the size of the integrated strain depends on the order of local accuracy of the numerical method suggests, as demonstrated in this paper, that such information can be used to verify not only that the method has been properly formulated but also that the algorithm is performing correctly. In light with this, the anticipated knowledge of the order of local accuracy of the numerical method to be used is employed in this paper to assess the importance of consistently updating all the variables involved in the numerical integration of the stress-strain relationships. In particular, in the context of the modified Cam clay model of Roscoe and Burland [21], the correct update of the specific volume plays a crucial role on the accuracy of the numerical solution and this is demonstrated in the paper by investigating the error incurred by two different substepping strategies (the second order modified Euler and

the fifth order Runge-Kutta-Dormand-Prince schemes with substepping) during the integration of the mechanical relations.

Finally, the information regarding the known order of local accuracy of the numerical method is also used in the paper to propose a new form of plotting the numerical outcomes of the explicit substepping algorithms with automatic error control and its effectiveness is demonstrated for various axisymmetric compression paths.

## STRESS-STRAIN RELATIONSHIPS

This section gives a brief summary of the equations involved in the elasto-plastic integration of critical state constitutive models for saturated soils with a hardening law depending on plastic volumetric strains. The notation adopted generally follows that employed by [3] but makes explicit the dependence of the response on the specific volume  $v$ . As demonstrated later, a consistent update of the specific volume  $v$  when integrating a critical state model becomes important in numerical methods whose order of accuracy is larger than one and, although often missed in the literature, such dependence of the problem on  $v$  should be included in the formulation. It is worth mentioning here that, in general, equivalent comments should apply to the explicit integration of more advanced constitutive models as, for example, those used for unsaturated soils, in which the consistent update of all internal variables involved in the constitutive model, such as the degree of saturation or bonding variables, will play a key role in the accuracy of the solution.

In this context, the mechanical behaviour of a saturated soil can be characterized by the following ordinary differential equation (ODE) (the superior dot represents a derivative with respect to time):

$$\dot{\boldsymbol{\sigma}}' = \mathbf{D}\dot{\boldsymbol{\varepsilon}} \quad (1)$$

where  $\dot{\boldsymbol{\sigma}}'$  is a vector of effective stress rate components (defined as the difference between the total stress and pore water pressure rates),  $\dot{\boldsymbol{\varepsilon}}$  is a vector of strain rate components, and  $\mathbf{D}$  is the elastic matrix  $\mathbf{D}_e$  (if no plastic yielding occurs) or the elasto-plastic matrix  $\mathbf{D}_{ep}$  when the given strain increment causes plastic yielding (see the

Appendix for the specific forms of  $\mathbf{D}_e$  and  $\mathbf{D}_{ep}$ ). If plastic yielding occurs, an additional ODE needs to be solved accounting for the evolution of the yield surface:

$$\dot{H} = \dot{\lambda}B \quad (2)$$

where  $\dot{H}$  is the rate of the hardening parameter (in the context of critical state models it usually corresponds to the pre-consolidation pressure  $p_0'$ ),  $\dot{\lambda}$  is an unknown scalar often referred to as the plastic multiplier, and  $B$  is a scalar function for the evolution of the yield surface during yielding (see the Appendix).

For critical state models the elastic/elasto-plastic matrices are typically assumed to depend on the tangential bulk modulus  $K$  which, in turn, is assumed to depend on the mean effective stress  $p'$  and specific volume  $v$ :

$$K = \frac{dp'}{d\varepsilon_v^e} = \frac{vp'}{\kappa} \quad (3)$$

where  $\varepsilon_v^e$  is the elastic volumetric strain and  $\kappa$  is the slope of the unload/reload line on the  $v$ :  $\ln p'$  plane.

In addition to the tangential bulk modulus  $K$ , the elastic/elasto-plastic matrices  $\mathbf{D}_e$  and  $\mathbf{D}_{ep}$  also depend on the elastic shear modulus  $G$  (see Appendix).  $G$  can either be assumed constant, or it can be calculated from the variable elastic tangential bulk modulus  $K$  by the assumption of a constant value of Poisson's ratio  $\nu$ :

$$G = \frac{3(1-2\nu)vp'}{2(1+\nu)\kappa} = \frac{3(1-2\nu)K}{2(1+\nu)} \quad (4)$$

Although the use of a variable elastic shear modulus of the form shown in Equation 4 is not strictly acceptable from a theoretical point of view (because it leads to the generation of deviatoric strain for certain types of closed stress path, [22] Zytynski *et al.* [22]) it often gives better fits with experimental data than a constant value of  $G$  [23].

Alternatively to the use of  $K$  and  $G$ , the elastic/elasto-plastic matrices can be expressed in terms of the secant bulk and secant shear moduli  $\bar{K}$  and  $\bar{G}$  respectively. The use of

$\bar{K}$  and  $\bar{G}$  in an explicit integration scheme is needed to compute the correct stress state at the intersection with the yield surface when the stress point passes from an elastic to a plastic state (Sheng *et al.*, [22]), because an analytical expression for  $\bar{K}$  (and, equivalently, also for  $\bar{G}$  if a constant value of Poisson's ratio is assumed, see Equation 4) can be found by integrating Equation 3 for  $p'$  and  $\varepsilon_v^e$  in combination with the definition of specific volume in terms of volumetric strain (see Appendix):

$$\bar{K} = \frac{p_{l=0}}{\Delta\varepsilon_v^e} \left[ \exp \left( \frac{v_{l=0} \left( 1 - \exp(-\Delta\varepsilon_v^e) \right)}{\kappa} \right) - 1 \right] \quad (5)$$

where  $p_{l=0}$  and  $v_{l=0}$  are the mean effective stress and specific volume, respectively, at the start of the volumetric strain increment  $\Delta\varepsilon_v^e$ . The expression for  $\bar{K}$  varies slightly from that presented in [3] because it is not assumed here that  $dv = \Delta v$  (see Appendix). The secant shear modulus  $\bar{G}$  can be computed from Equation 4 by inserting  $\bar{K}$  to replace  $K$ . It is important to emphasize that the elastic matrix forms considered here (and, in turn, the elasto-plastic matrix) depend not only on the current value of the mean effective stress  $p'$  but also on the current value of the specific volume  $v$  (see Appendix). Consequently, the update of  $p'$  in the numerical method to solve Equations 1 and 2 should be in agreement with the update for  $v$ . Such consistency avoids a potential source of error and is described in the following.

## EXPLICIT SUBSTEPPING FORMULATION FOR CRITICAL STATE MODELS

This section summarises the substepping strategy with automatic error control to solve the system of ordinary equations (ODE) defined by Equations 1 and 2. Full description of the algorithm including the numerical aspects of how to handle elastic-plastic transitions, yield surface intersections and correction of stresses back to the yield surface (see Potts & Gens [25]) is given in [3].

In the formulation of a substepping algorithm, it is useful to consider a pseudo-time  $T$ , defined by:

$$T = \frac{(t - t_0)}{\Delta t} \quad (6)$$

where  $t = t_0$  is the time at the start of the strain increment  $\Delta \boldsymbol{\varepsilon}$  (i.e.  $T = 0$ ),  $t = t_0 + \Delta t$  is the time at the end of the strain increment (i.e.  $T = 1$ ) and  $0 \leq T \leq 1$ . Equations 1 and 2 can be expressed in terms of the pseudo-time  $T$  (note that in the following equations, the superscript  $T$  denotes transposed):

$$\frac{d\boldsymbol{\sigma}'}{dT} = \mathbf{D}_{ep} \Delta \boldsymbol{\varepsilon} = \Delta \boldsymbol{\sigma}'_e - \Delta \lambda \mathbf{D}_e \mathbf{b} \quad (7)$$

$$\frac{dH}{dT} = \dot{\lambda} \Delta t B = \Delta \lambda B \quad (8)$$

where,

$$\Delta \lambda = \frac{\mathbf{a}^T \mathbf{D}_e \Delta \boldsymbol{\varepsilon}}{A + \mathbf{a}^T \mathbf{D}_e \mathbf{b}} = \frac{\mathbf{a}^T \Delta \boldsymbol{\sigma}'_e}{A + \mathbf{a}^T \mathbf{D}_e \mathbf{b}} \quad (9)$$

where  $\mathbf{a}$  and  $\mathbf{b}$  are vectors giving, respectively, the derivatives of the yield surface and plastic potential with respect to effective stress and  $A$  is a scalar containing information on the hardening law (see Appendix). The system of ODEs specified by Equations 7 and 8 define an initial value problem (IVP) that can be integrated over  $T$  knowing the initial effective stresses  $\boldsymbol{\sigma}'$ , initial hardening parameter  $H_0$  and initial specific volume  $v_0$  at  $T = 0$  (or, equivalently, the intercept  $N$  of the saturated normal compression line), together with the imposed strain increment  $\Delta \boldsymbol{\varepsilon}$  ( $\Delta \boldsymbol{\varepsilon}$  are the fixed strains to be integrated over  $\Delta t$ ). Equations 7-9 depend on the specific volume and, as such,  $v$  may vary within the substepping integration of  $\Delta \boldsymbol{\varepsilon}$  (in addition to  $\boldsymbol{\sigma}'$  and  $H$ ). This variation in  $v$  influences both  $d\boldsymbol{\sigma}'$  and  $dH$  through the elastic matrix  $\mathbf{D}_e$  and the scalar functions  $A$  and  $B$ .

#### *Modified Euler scheme with substepping*

As detailed in [3], the modified Euler (ME) with substepping estimates the relative local error by taking the difference between the first order accurate forward Euler and the second order accurate modified Euler approximations for the effective stresses (and hardening parameter) and dividing this difference by the corresponding higher order

approximation. This relative measure of the local error (i.e. *REL*) is used to automatically adjust the size of the integration step, by reducing/increasing its current size (i.e. substepping) when *REL* is larger/smaller than a specified tolerance (i.e. *STOL*). Such a criterion for adjusting the step size is known as *error per step* EPS and, when the update of the integrated variables after a successful step is carried out using the higher order approximation (an approach called *local extrapolation*), the criterion is typically referred to as XEPS (Shampine [26]). Local extrapolation is adopted in [3] and also followed here.

Given a pseudo-time step/substep  $\Delta T_n$  with  $0 < \Delta T_n \leq 1$ , the forward Euler updates for  $\boldsymbol{\sigma}'$  and  $H$  are (with the subscripts  $n-1$  and  $n$  denote quantities evaluated at pseudo-times  $T_{n-1}$  and  $T_n = T_{n-1} + \Delta T_n$  respectively) :

$$\boldsymbol{\sigma}'_n = \boldsymbol{\sigma}'_{n-1} + \Delta \boldsymbol{\sigma}'_1 \quad (10)$$

$$H_n = H_{n-1} + \Delta H_1 \quad (11)$$

$$v_n = v_{n-1} \exp(-\Delta T_n \Delta \varepsilon_v) \quad (12)$$

where,

$$\Delta \boldsymbol{\sigma}'_1 = \mathbf{D}_{\text{ep}}(\boldsymbol{\sigma}'_{n-1}, H_{n-1}, v_{n-1}) \Delta \boldsymbol{\varepsilon}_n \quad (13)$$

$$\Delta H_1 = \Delta \lambda(\boldsymbol{\sigma}'_{n-1}, H_{n-1}, v_{n-1}, \Delta \boldsymbol{\varepsilon}_n) B(\boldsymbol{\sigma}'_{n-1}, v_{n-1}) \quad (14)$$

and

$$\Delta \boldsymbol{\varepsilon}_n = \Delta T_n \Delta \boldsymbol{\varepsilon} \quad (15)$$

The inclusion of  $v_{n-1}$  in the forward Euler update of  $\boldsymbol{\sigma}'$  and  $H$  makes the dependence of the elastoplastic relations on  $v$  explicit, whilst also accounting for the dependency on  $\boldsymbol{\sigma}'$  and  $H$ . Assuming that  $\Delta \boldsymbol{\varepsilon}$  is known, the value of the specific volume at the end of the step/substep given by Equation 12 is exact because it is possible to integrate the volumetric strains analytically over  $\Delta T_n$  to find the precise value of  $v$  at  $n$ . The

corresponding second order accurate updates for  $\boldsymbol{\sigma}'$  and  $H$ , and exact update for  $v$ , are given by:

$$\hat{\boldsymbol{\sigma}}'_n = \boldsymbol{\sigma}'_{n-1} + \frac{1}{2} \Delta \boldsymbol{\sigma}'_1 + \frac{1}{2} \Delta \boldsymbol{\sigma}'_2 \quad (16)$$

$$\hat{H}_n = H_{n-1} + \frac{1}{2} \Delta H_1 + \frac{1}{2} \Delta H_2 \quad (17)$$

$$\hat{v}_n = v_{n-1} \exp(-\Delta T_n \Delta \varepsilon_v) \quad (18)$$

where  $\Delta \boldsymbol{\sigma}'_1$  and  $\Delta H_1$  are computed using the forward Euler update (Equations 13 and 14, respectively) and

$$\Delta \boldsymbol{\sigma}'_2 = \mathbf{D}_{ep}(\boldsymbol{\sigma}'_n, H_n, v_n) \Delta \boldsymbol{\varepsilon}_n \quad (19)$$

$$\Delta H_2 = \Delta \lambda(\boldsymbol{\sigma}'_n, H_n, v_n, \Delta \boldsymbol{\varepsilon}_n) B(\boldsymbol{\sigma}'_n, v_n) \quad (20)$$

with  $\boldsymbol{\sigma}'_n$ ,  $H_n$  and  $v_n$  being computed using the forward Euler update (Equations 10-12).

If the step/substep is accepted, the values of the effective stresses  $\hat{\boldsymbol{\sigma}}'_n$  and hardening parameter  $\hat{H}_n$  at  $n$  (end of the step/substep) are updated using the higher order approximation with the elasto-plastic matrix  $\mathbf{D}_{ep}$  computed using the appropriate specific volume, consistent with all the other variables as shown in Equations 13, 14, 19 and 20. Similar comments also apply to the update of the hardening parameter (Equations 14 and 20).

#### *Runge-Kutta-Dormand-Prince scheme with substepping*

The explicit Runge-Kutta-Dormand-Prince (RKDP) with substepping estimates the relative local error (*REL*) by taking the difference between the approximations for the stresses (and hardening parameter) given by fourth and fifth order accurate schemes, and then dividing this quantity by the fifth order approximation. This estimate is then compared against *STOL* to adjust the size of the integration step as discussed for the ME case. This integration scheme results in very accurate values for  $\boldsymbol{\sigma}'_n$  and  $H_n$  at the

end of each step/substep at the expense of additional evaluations of the constitutive relations. In the absence of an analytical solution, the highly accurate 5<sup>th</sup> order RKDP approximations can be used as a *reference* to check the accuracy of lower order methods as discussed in [3] and demonstrated in the next sections. Applying this scheme to Equations 7 and 8, the fourth and fifth order accurate approximations for  $\boldsymbol{\sigma}'$  and  $H$ , together with the exact updates for  $v$ , at the end of a pseudo-time step/substep  $\Delta T_n$  are given by:

$$\boldsymbol{\sigma}'_n = \boldsymbol{\sigma}'_{n-1} + \frac{31}{540} \Delta \boldsymbol{\sigma}'_1 + \frac{190}{297} \Delta \boldsymbol{\sigma}'_3 - \frac{145}{108} \Delta \boldsymbol{\sigma}'_4 + \frac{351}{220} \Delta \boldsymbol{\sigma}'_5 + \frac{1}{20} \Delta \boldsymbol{\sigma}'_6 \quad (21)$$

$$H_n = H_{n-1} + \frac{31}{540} \Delta H_1 + \frac{190}{297} \Delta H_3 - \frac{145}{108} \Delta H_4 + \frac{351}{220} \Delta H_5 + \frac{1}{20} \Delta H_6 \quad (22)$$

$$v_n = v_{n-1} \exp(-\Delta T_n \Delta \varepsilon_v) \quad (23)$$

and

$$\hat{\boldsymbol{\sigma}}'_n = \boldsymbol{\sigma}'_{n-1} + \frac{19}{216} \Delta \boldsymbol{\sigma}'_1 + \frac{1000}{2079} \Delta \boldsymbol{\sigma}'_3 - \frac{125}{216} \Delta \boldsymbol{\sigma}'_4 + \frac{81}{88} \Delta \boldsymbol{\sigma}'_5 + \frac{5}{56} \Delta \boldsymbol{\sigma}'_6 \quad (24)$$

$$\hat{H}_n = H_{n-1} + \frac{19}{216} \Delta H_1 + \frac{1000}{2079} \Delta H_3 - \frac{125}{216} \Delta H_4 + \frac{81}{88} \Delta H_5 + \frac{5}{16} \Delta H_6 \quad (25)$$

$$\hat{v}_n = v_{n-1} \exp(-\Delta T_n \Delta \varepsilon_v) \quad (26)$$

where

$$\left. \begin{aligned} \Delta \boldsymbol{\sigma}'_i &= \mathbf{D}_{\text{ep}}(\tilde{\boldsymbol{\sigma}}'_i, \tilde{H}_i, \tilde{v}_i) \Delta \boldsymbol{\varepsilon}_n \\ \Delta H_i &= \Delta \lambda(\tilde{\boldsymbol{\sigma}}'_i, \tilde{H}_i, \tilde{v}_i, \Delta \boldsymbol{\varepsilon}_n) B(\tilde{\boldsymbol{\sigma}}'_i, \tilde{v}_i) \\ \Delta \boldsymbol{\varepsilon}_n &= \Delta T_n \Delta \boldsymbol{\varepsilon} \end{aligned} \right\} \text{ for } i = 1, 2, \dots, 6 \quad (27)$$

and

$$\left. \begin{aligned} \tilde{\sigma}'_1 &= \sigma'_{n-1} \\ \tilde{H}_1 &= H_{n-1} \\ \tilde{v}_1 &= v_{n-1} \end{aligned} \right\} \quad (28)$$

$$\left. \begin{aligned} \tilde{\sigma}'_2 &= \sigma'_{n-1} + \frac{1}{5} \Delta \sigma'_1 \\ \tilde{H}_2 &= H_{n-1} + \frac{1}{5} \Delta H_1 \\ \tilde{v}_2 &= v_{n-1} \exp\left(-\frac{1}{5} \Delta T_n \Delta \varepsilon_v\right) \end{aligned} \right\} \quad (29)$$

$$\left. \begin{aligned} \tilde{\sigma}'_3 &= \sigma'_{n-1} + \frac{3}{4} \Delta \sigma'_1 + \frac{9}{40} \Delta \sigma'_2 \\ \tilde{H}_3 &= H_{n-1} + \frac{3}{4} \Delta H_1 + \frac{9}{40} \Delta H_2 \\ \tilde{v}_3 &= v_{n-1} \exp\left\{-\left(\frac{3}{4} + \frac{9}{40}\right) \Delta T_n \Delta \varepsilon_v\right\} \end{aligned} \right\} \quad (30)$$

$$\left. \begin{aligned} \tilde{\sigma}'_4 &= \sigma'_{n-1} + \frac{3}{10} \Delta \sigma'_1 - \frac{9}{10} \Delta \sigma'_2 + \frac{6}{5} \Delta \sigma'_3 \\ \tilde{H}_4 &= H_{n-1} + \frac{3}{10} \Delta H_1 - \frac{9}{10} \Delta H_2 + \frac{9}{40} \Delta H_3 \\ \tilde{v}_4 &= v_{n-1} \exp\left\{-\left(\frac{3}{10} - \frac{9}{10} + \frac{9}{40}\right) \Delta T_n \Delta \varepsilon_v\right\} \end{aligned} \right\} \quad (31)$$

$$\left. \begin{aligned} \tilde{\sigma}'_5 &= \sigma'_{n-1} + \frac{226}{729} \Delta \sigma'_1 - \frac{25}{27} \Delta \sigma'_2 + \frac{880}{729} \Delta \sigma'_3 + \frac{55}{729} \Delta \sigma'_4 \\ \tilde{H}_5 &= H_{n-1} + \frac{226}{729} \Delta H_1 - \frac{25}{27} \Delta H_2 + \frac{880}{729} \Delta H_3 + \frac{55}{729} \Delta H_4 \\ \tilde{v}_5 &= v_{n-1} \exp\left\{-\left(\frac{226}{729} - \frac{25}{27} + \frac{880}{729} + \frac{55}{729}\right) \Delta T_n \Delta \varepsilon_v\right\} \end{aligned} \right\} \quad (32)$$

$$\left. \begin{aligned} \tilde{\sigma}'_6 &= \sigma'_{n-1} - \frac{181}{270} \Delta \sigma'_1 + \frac{5}{2} \Delta \sigma'_2 - \frac{226}{297} \Delta \sigma'_3 - \frac{91}{27} \Delta \sigma'_4 + \frac{189}{55} \Delta \sigma'_5 \\ \tilde{H}_6 &= H_{n-1} - \frac{181}{270} \Delta H_1 + \frac{5}{2} \Delta H_2 - \frac{226}{297} \Delta H_3 - \frac{91}{27} \Delta H_4 + \frac{189}{55} \Delta H_5 \\ \tilde{v}_6 &= v_{n-1} \exp\left\{-\left(-\frac{181}{270} + \frac{5}{2} - \frac{226}{297} - \frac{91}{27} + \frac{189}{55}\right) \Delta T_n \Delta \varepsilon_v\right\} \end{aligned} \right\} \quad (33)$$

## PERFORMANCE OF INTEGRATION SCHEMES

This section studies the behaviour of the local error when numerically integrating the stress-strain relationships of critical state constitutive models. The study involves a comparison, for a specified problem, of the approximations given by various explicit integration schemes with and without substepping. To assess the error incurred by each integration scheme, the corresponding approximations for (effective) stresses are compared against an analytical solution (or a reference approximation if needed).

In general, two primary sources of error exist in a numerical solution of an IVP: the error that relates to the precision of the computer/machine to perform the calculations (rounding error) and the local truncation error incurred by the numerical method. This work relates only to the truncation (relative) error which is quantified in a manner which is consistent with the way the local error is controlled in the substepping strategy. Following [3], the relative local error in the stresses can be computed from:

$$REL = \frac{\left\{ (\boldsymbol{\sigma}'_{ref} - \boldsymbol{\sigma}')^T (\boldsymbol{\sigma}'_{ref} - \boldsymbol{\sigma}') \right\}^{1/2}}{\left\{ (\boldsymbol{\sigma}'_{ref})^T (\boldsymbol{\sigma}'_{ref}) \right\}^{1/2}} \quad (34)$$

where  $\boldsymbol{\sigma}'_{ref}$  is the reference (or analytical) solution and  $\boldsymbol{\sigma}'$  is the numerical approximation. The numerical approximation here is found from the numerical integration of a single strain increment (input), the size of which is varied in each simulation. To minimise the influence of rounding error, a lower-bound on the value of the local error investigated is set in the range  $10^{-12}$  and  $10^{-13}$ . This lower-bound is considered suitable for the numerical results presented, as double precision real variables in FORTRAN® with 15 significant digits were used. Note that the numerator of Equation 34 can be used for analyses which aim to measure the absolute error. In these cases, it is important, for consistency, that the numerical approximations are computed by a substepping algorithm that also controls the absolute error in the stresses (i.e. the denominator is set to unity in Equation 34 when computing *REL*).

Three analyses are carried out, all adopting the modified Cam clay model (MCC) of [21] and assuming axisymmetric conditions. All three analyses assume an initial stress state on the yield surface with zero deviatoric stress. The soil constants and initial state

considered in all the simulations are summarised in Table 1, where  $N$  and  $\lambda$  are respectively the intercept at  $p' = 1$  kPa and the gradient of the NCL in the  $v:\ln p'$  plane. The tolerance associated with the yield surface intersection and the correction of the stresses back to the yield surface,  $FTOL$ , is assumed equal to  $10^{-12}$  and the maximum number of substeps is limited to  $10^{+06}$  in all the analyses. The values considered for  $STOL$  vary from 1 to  $10^{-08}$ .

In the first analysis, the local error is calculated using Equation 34 with the correct/analytical solution for an isotropic loading increment together with the corresponding numerical approximation obtained by the integration scheme considered. Conversely, the second and third analyses use Equation 34 to compare the numerical approximation against a reference solution (obtained by using the RKDP scheme with substepping and very stringent tolerances) for an axial loading increment (with no radial strains) and for an undrained shear loading increment, respectively. In all analyses, the size of the assumed strain increment is varied to study how this influences the error in the solution. For the isotropic and zero radial strain loadings, the strain increment size analysed varies from  $\Delta\varepsilon_v = 10^{-06}$  to 0.1, corresponding to a maximum variation in the sample volume of 10%. For the case of undrained shear loading, the axial strain analysed varies from  $\Delta\varepsilon_a = 10^{-06}$  to 0.01, corresponding to a maximum sample height reduction of 1%.

#### *Consistent update of specific volume in an integration scheme*

Probably the clearest comparison between different integration schemes is to consider the solution for stresses approximated by each numerical method for a single elasto-plastic isotropic loading increment starting at a known initial isotropic stress state A on the yield surface. The simplicity of this stress path is chosen because, in the context of the MCC model, it corresponds to stress states lying on the saturated normal compression line (NCL) and, hence, exact values of the effective stress under axisymmetric conditions for any given increment of volumetric strain  $\Delta\varepsilon_v$  can be found (see Appendix), provided that the initial values of the effective stress  $\sigma'_A$  ( $\sigma'_r = \sigma'_a = p'_A$ , where  $\sigma'_r$  and  $\sigma'_a$  are the radial and axial effective stress respectively) and the specific volume  $v_A$  are also known, together with the model parameter values (Table 1). The example provides a clear and unambiguous quantification of the errors in the computed solution for  $\sigma'$  at the end of the step for each integration scheme when the size of  $\Delta\varepsilon_v$  is

varied because, in addition to the comments above, no correction of the stresses back to the yield surface (drift correction) was needed for the strain step sizes considered, which does not cloud the interpretation of the errors measured.

The local truncation error refers, hereafter, to the error incurred by the numerical scheme in a single substep (or step in the case of no substepping) whereas the global error is interpreted as the local error accumulated over a number of substeps. In this context, it is important to note that the error control in the substepping strategy only controls the local truncation error (in a single substep), with the aim of controlling the global error over many steps. The effectiveness of this technique can be measured by comparing the computed solution with the exact solution for a variety of imposed strains.

To assess the accuracy and convergence of each numerical method, the local error in stresses is plotted against the size of the volumetric strain using logarithmic scales. This facilitates a partial verification of the substepping strain-driver algorithm because, by definition, the gradient obtained for the best-fitted straight line through a particular set of results (i.e. all belonging to approximations from the same integration scheme) should correspond to the order of accuracy of the numerical integration method. This follows from the fact that a numerical method has order of accuracy  $p$  if the local truncation error  $e$  (i.e. the error incurred in a single step of the integration scheme) is  $O(h^{p+1})$  for  $h$  sufficiently small, where  $h$  is the step/substep size being integrated and  $O(h^{p+1})$  refers to those terms of the Taylor's series expansion of order higher than  $p$ . Interestingly, for a sufficiently small value of  $h$ ,  $O(h^{p+1}) \cong ch^{p+1}$  (where  $c$  is a constant) and, hence, when plotting  $e$  against  $h$  on a log-log scale the gradient observed should be approximately  $p + 1$  [26].

In addition to the ME and RKDP schemes with substepping introduced earlier, four other single step explicit integration methods (without substepping) are considered in the analysis to support the discussion: the first order forward Euler (FE 1st) scheme, the second order modified Euler scheme (ME 2nd), and the fourth and fifth order Runge-Kutta-Dormand-Prince schemes (RKDP4 and RKDP5, respectively). Each of these schemes is formulated in a strain-driven algorithm following two different

approaches: (i) updating the specific volume only at the end of the step, and (ii) updating the specific volume consistently with all the other variables involved.

Note that updating the specific volume only at the end of the step  $n$  (using the analytical solution given by Equation 12) also provides the correct value of the specific volume at step  $n$ , because the strain increment considered is assumed to be known/correct. However, in such a case, the incurred local error in the updated stresses (and hardening parameter) may be larger than that which corresponds to the theoretical order of accuracy of the numerical method used. In other words, the order of accuracy of the numerical scheme is reflected in how the error responds to changes in the size of  $h$ . As demonstrated in the following, this information can be used not only to verify the correctness of the algorithmic formulation but also to check and discuss its performance.

Table 2 shows the relative local errors incurred by single step explicit integration schemes (with no substepping) when the specific volume is updated only at the end of a given step size. Table 3 shows equivalent computations for the case where the specific volume is updated consistently with the effective stress and hardening parameter during the integration of the strain increment. The results from these two tables are illustrated in Figures 1a and 1b respectively.

Inspection of Figure 1a shows a number of inconsistencies in the results from the algorithms in which the specific volume is updated only at the end of the step. Even though all the simulations plotted in this Figure show linear convergence (i.e. the relative local error in the stresses decreases linearly with decreasing step size) they do not converge at the expected rate (i.e. the decrease in error for a given decrease in  $\Delta\varepsilon_v$  is less than expected). In fact, in Figure 1a, the best-fit straight line for the first order forward Euler scheme (indicated by the thicker dashed line) is roughly parallel to the results for the other integration schemes. This suggests that the order of accuracy achieved by the ME, RKDP4 and RKDP5 schemes is approximately the same as that for a first order accurate scheme (i.e. having a gradient of two). In contrast Figure 1b, which shows results for the case where the specific volume is updated consistently with the effective stress and hardening parameter, has error plots whose gradients match the expected order of accuracy of the numerical method. For example, a gradient of 5 is obtained when best-fitting a straight line through the computed error values

corresponding to the RKDP4 method. Note that the inconsistencies in Figure 1a are evident only for methods with an order higher than one because, when using the first order forward Euler method, the update of  $v$  is always carried out at the end of the step.

Another interesting feature illustrated in Figure 1b is how the vertical distance between the different best-fitted straight lines varies with the size of imposed strain increment. In particular, the vertical distance between the best-fit lines for the first and second order Euler schemes (or, similarly, for the RKDP4 and RKDP5 schemes) may be used to assess the likely influence that the error tolerance *STOL* would have in the computations with a substepping scheme. In general, for a given step size, a large number of substeps will be required to fulfil a stringent *STOL* when the vertical distance between the two methods involved in the substepping is large. Conversely, if the vertical spacing is small (relative to the specified *STOL*) only a few (or no) substeps will be activated during the integration. Indeed, for these cases, a stringent value of *STOL* will be required to improve the accuracy of the solution compared to that which is achievable from a single step integration using the highest order method. In light of this, the results shown in Figure 1a indicate a major potential problem with the RKDP sub-stepping schemes when the specific volume is not updated consistently with the effective stress and hardening parameter during the integration process. Not only are the solutions shown in Figure 1a extremely close for both the RKDP4 and RKDP5 schemes, but they also correspond to first order accurate approximations (and not the fourth and fifth order approximations that they should be).

To investigate also how the error behaves in the substepping schemes (in addition to the conventional one step schemes studied above) the integration of one single volumetric strain increment of 0.1 is analysed by using the ME and RKDP schemes with substepping for three different values of *STOL*. The different values of *STOL* considered ( $10^{-04}$ ,  $10^{-06}$  and  $10^{-08}$ ) correspond to Figures 2, 3 and 4 respectively. Parts a (Figures 2a, 3a and 4a) plot the substepping approximations with no update of  $v$  during each substep (i.e.  $v$  is only updated at the end of the entire increment) whereas parts b (Figures 2b, 3b and 4b) show the approximations from the same integration schemes but updating  $v$  consistently throughout the substepping. Note that the values of relative error plotted in the figures, correspond to the accumulated contributions of local error at each substep and, hence, represent the global error behaviour. Consequently, at the

end of the substepping, the sum of all the substep sizes integrated should be equal to the volumetric strain increment prescribed 0.1. The previously best-fitted straight lines in Figures 1a and 1b have been also included in the plots to provide a reference for the discussion.

Tables 4 and 5 present the global errors incurred by the substepping schemes to integrate the imposed volumetric strain increment of 0.1 for  $STOL = 10^{-04}$ ,  $10^{-06}$  and  $10^{-08}$ . The results in Table 4 correspond to substepping schemes without update of  $\nu$  during the substepping whereas Table 5 shows approximations given by substepping schemes with a consistent update of  $\nu$ . In the tables, the total number of substeps required in the algorithm is indicated by TS whereas the total number of failed substeps (substeps requiring a further subdivision in size) is indicated by TF. For the elasto-plastic isotropic loading considered, no drift correction of the stresses back to the yield surface was needed.

As expected, more accurate approximations are obtained when using more stringent tolerances, and these typically involve a larger number of substeps (see Tables 4 and 5). The arrows in Figures 2 to 4 indicate the *optimal* strain size at which the substepping is performed. When updating  $\nu$  correctly, this optimal size approximately corresponds to the intersection between the considered value of  $STOL$  and the best-fitted line for the lower order scheme within the substepping algorithm (which, in turn, corresponds to the dominant term of the local error). For strain increment sizes smaller than that indicated by the arrows in Figures 2, 3 and 4 no substepping is performed. In such cases, the accuracy of the solutions converges to that from the highest order single step method used in the corresponding substepping algorithm. As expected, the increment size below which no substepping is needed decreases with decreasing values of  $STOL$  (see Figures 2, 3 and 4).

During the numerical integration of  $\Delta\varepsilon_v = 0.1$ , the actual substep size being integrated is quite regular in all the schemes considered. Consequently, a roughly vertical increase of the global error during the integration is observed in Figures 2, 3 and 4. There is often one single substep size considerably smaller than the other the sizes used by the algorithm corresponding to the last remaining part for the full integration of  $\Delta\varepsilon_v = 0.1$  (this has almost no influence on the final global error).

Figures 2a, 3a and 4a show the substepping schemes that only update  $v$  at the end of the given step successfully control the error, but the error response is not in agreement with the expected gradients of the numerical method used (see earlier comments on Figure 1a). Not surprisingly, the ME with substepping scheme without the correct update of  $v$  achieves, in general, more accurate results than the RKDP substepping scheme in Figures 2a, 3a and 4a. This is a direct consequence of the larger vertical distances observed between the forward Euler and ME approximations in Figure 1a, compared with their RKDP counterparts.

Figures 2b, 3b and 4b show that the solutions are more accurate than those above when the correct update for update for  $v$  is employed. As indicated in Tables 4 and 5, this increase in accuracy is achieved with a similar number of failed substeps (TF) and without increasing the number of substeps (TS).

Some useful information underlying the vertical response of the global error should be further discussed. In general, the global error,  $E$ , incurred by a substepping scheme is the result of adding each amount of local truncation error  $e$  incurred in each substep (assuming no cancellation). For sufficiently small step sizes  $h$ , it was shown that  $e \cong O(h^{p+1}) \cong ch^{p+1}$  and, consequently, for  $n$  equal-sized  $h$ , the global error can be approximated by  $E \cong nch^{p+1} \cong Hch^p$ , where  $H$  is the total strain increment size integrated and  $n$  is the total number of substeps used to integrate  $H$ . This means that, for approximately equal sized  $h$  (as it is the case in Figures 2, 3 and 4) the final global error (for this particular value of  $h$ ) should lie on a straight line when plotted in a log-log scale, having gradient 2 and 4 for the ME and RKDP with substepping schemes respectively. Furthermore, the intercepts of these global error lines are  $Hc$  where  $c$  is the intercept of the best-fitted line for the higher order method approximations. This means that the distance between the best-fitted straight line for the higher order scheme (i.e.  $O(h^{p+1}) \cong ch^{p+1}$ ) and one of these global error lines is (at a particular  $h$ )  $h/H$  or, equivalently,  $1/n$ . This type of response is illustrated in Figure 3 for three different values of  $H = 0.1, 0.01$  and  $0.001$ , when using the ME with substepping and is further discussed in the next section.

The values of the global error at the end of the integration of the entire volumetric strain considered (i.e. 0.001, 0.01 or 0.1) are indicated in Figure 3 by a light-grey symbol.

When using the ME substepping scheme with the correct update of the specific volume, 10 substeps are needed to integrate the volumetric strain size of 0.001, 96 for 0.01 and 910 for 0.1 (Figure 3b). In such cases, the final value of global error resulting from the integration of the corresponding number of substeps converge to a point lying, in fact, on a straight line of gradient two as indicated in Figure 3b by a chain-dotted line. This means that the order of accuracy of the global error in the ME method with substepping and the consistent update of  $v$  is one order lower than the accuracy of its local truncation error (see the parallel lines in Figure 3). It is interesting to verify that the distances between these chain-dotted parallel lines and the best-fitted straight line for the single step ME scheme are indeed equal to  $1/n$  for each particular  $H$  as discussed above. In contrast, Figure 3a show equivalent results but using the ME with substepping with an incorrect update of  $v$ . As discussed earlier, the computations from this method result, incorrectly, in a first order local error (see Figure 1a) and, consequently, the accumulated first order local error (over the imposed  $H$ ) leads to a global error of one order of accuracy less (demonstrating that the substepping strategy itself is performing correctly even though the incorrect update of  $v$  leads to imprecise approximations having one order of accuracy less than expected). Indeed, when using the ME substepping scheme without a consistent update of  $v$ , 10 substeps are needed to integrate the volumetric strain size of 0.001, 100 for 0.01 and 950 for 0.1 (Figure 3a). In these cases, the final value of the global error resulting from the integration of the corresponding number of substeps also converges to a point lying on a straight line (also indicated by a chain-dotted line), but having now a gradient of one (Figure 3a). This is agreement with the reduction in order of the global error just mentioned but in disagreement with the expected order of accuracy of this method.

### *Error behaviour and numerical performance*

Now that the importance of updating consistently the specific volume during the numerical integration of the stress-strain relations of the MCC has been demonstrated, the next analyses concentrate only on approximations from numerical schemes that update  $v$  correctly. The computational aspects for the isotropic loading conditions are discussed first followed by the analyses involving axial loading at zero lateral strains and shearing under undrained loading conditions.

Figures 5 and 6 show a complete picture of the error behaviour when numerically integrating the MCC mechanical relationships for isotropic stress paths involving different volumetric strain loads. Approximations given by the ME with substepping are plotted in Figure 5 whereas the substepping RKDP solutions are presented in Figure 6.

These forms of plotting the results are suitable to assess how the local error propagates as the integration progresses for various values of  $STOL$ . As discussed in Figure 3, during a typical substepping integration of a prescribed strain size  $H$  with  $n$  substeps, the local error incurred in each of these substeps (all fulfilling the imposed  $STOL$ ) accumulates in subsequent iterations and such local error accumulation corresponds to the global error. Figures 5 and 6 show how these final values of accumulated local error (once the entire  $H$  has been integrated) approximately lie on a straight line of gradient two for the ME with substepping and four for the RKDP with substepping. This behaviour is true for all values of  $STOL$  used (Figures 5 and 6) and is consistent with the previous comments on Figure 3. There is remarkable consistency in the distances between each best fitted line through the global error results, showing good agreement between their intercepts and the inverse of the number of substeps used to integrate  $H$  for any prescribed  $STOL$ , in correspondence with earlier comments. These conclusions are less apparent in Figure 6a as a consequence of both the small number of substeps typically used in the RKDP scheme together with the high accuracy of the method (resulting in larger gradients and smaller distances between the best fitted lines).

Closer inspection of Figures 5a and 6a shows that, for the larger sizes of  $h$  plotted, the error response of the substepping scheme with  $STOL = 1$  diverges slightly from its corresponding best-fitted straight line. This result indicates that the earlier assumption of  $h$  being sufficiently small is not fulfilled and, consequently, for this value of  $h$  and larger the approximation  $O(h^{p+1}) \cong ch^{p+1}$  becomes less accurate. Not surprisingly, this affects the quality of the estimate for the local error used in the algorithm to accept or reject the step size  $h$ , and is illustrated in the figures by the progressive loss of verticality observed in the global error plots when  $h$  increases. Because of the higher accuracy of the method, the values of  $h$  at which this behaviour becomes more apparent are slightly larger for the RKDP substepping scheme (with an approximate value of  $h \cong 0.05$ ) than in the ME with substepping scheme ( $h \cong 0.02$ ).

Figure 7 shows the relative local error for stresses incurred in the same isotropic loading simulations discussed in Figures 5 and 6, but now plotted against the number of substeps required for the integration of the entire strain increment. Figure 8 plots the same relative local error against  $STOL$  for each integrated size of volumetric strain. In these figures, parts b indicate the results for the ME with substepping and parts b present their RKDP substepping counterparts.

A further verification of the correctness of the algorithmic formulation can be checked when plotting the relative local error against the number of substeps on a log-log scale. In the substepping methods described by [3], the size of the  $n + 1$  substep ( $h_{n+1}$ ) is assumed to vary proportionally to the size of the current step at  $n$  i.e.  $\Delta T_{n+1} \cong q \cdot \Delta T_n$  where  $q$  is estimated from the local order as follows. Given that the forward Euler approximations have a local truncation error  $O(h^2)$ , these are the dominant terms of the local error incurred when using the modified Euler with substepping. Consequently,  $REL_{n+1} \cong q^2 \cdot REL_n$  where  $REL$  is the measure of the local error estimated from the difference between the first and second order accurate approximations. Combining this constraint with the assumption in the substepping strategies that  $REL_{n+1} \leq STOL$  gives  $q \leq (STOL/REL_n)^{1/2}$ . Sloan *et al.* [3] suggests that a suitable choice for computing  $q$  in the ME with substepping is  $q \cong 0.9(STOL/REL_n)^{1/2}$ . Similarly, the RKDP with substepping adopts  $q \cong 0.9(STOL/REL_n)^{1/5}$ . As a consequence, the gradient of the best-fitted straight lines plotted in Figure 7 have an approximate negative gradient of -2 for the ME with substepping (Figure 7a) and -5 for the RKDP with substepping (Figure 7b).

Inspection of Figure 8 shows the influence of  $STOL$  in the relative local error. As expected, a reduction in the values of  $STOL$  leads to a reduction in the relative local error incurred in the computations. However, this reduction of the local error with decreasing  $STOL$  is limited for small sizes of volumetric strain and becomes almost negligible for the smallest step sizes considered in this analysis (Figure 8). As discussed earlier, this is because for small step sizes the difference between the two solutions of different order within the substepping scheme tends to be very small and, if it is less than the  $STOL$  considered, the substepping strategy is not activated. In fact, for a given volumetric strain step size of  $10^{-02}$ , values of  $STOL$  smaller than  $10^{-02}$  are required to activate the substepping strategy with the ME scheme (Point Y in Figure 8a). The

RKDP with substepping, on the other hand, needs values of  $STOL$  smaller than  $10^{-07}$  (Point Y in Figure 8b). Moreover, for the same volumetric strain size of  $10^{-02}$ , 952 substeps are required for the ME substepping scheme (with  $STOL = 10^{-08}$ ) to reach a relative local error of about  $10^{-10}$ . In contrast, for the RKDP substepping scheme, only 2 substeps are required to reach a similar (even slightly smaller) value of the relative local error (see Figure 8).

The specific form of plotting the results in Figures 7 and 8 provides an ideal platform to assess the computational performance of the substepping algorithms. They show not only how the error behaves but also how it is influenced by  $STOL$  and the number of substeps (or, similarly, the prescribed increment strain size). These *performance maps* are also very useful from a practical point of view, as they can be used to assess the value of  $STOL$  that is best suited to reach a prescribed level of accuracy while also anticipating the associated approximate computational cost.

Similar responses to those just discussed for isotropic loading conditions are also observed in the remaining figures covering axial loading with zero radial strains (Figures 9 and 10) and undrained shear stress paths (Figures 11 and 12). Even in the case of not using a correct solution to compute the local error, the error behaviour for axial loading under zero radial strain and undrained-shear conditions illustrated in their respective performance maps is consistent with that shown in the previous section for isotropic stress conditions. The similarities between both analyses provide support to the strategy of using such forms of plotting to check the performance of explicit algorithms and verify that, if a substepping strategy is used, the automatic error control is working correctly.

#### *Further computational aspects: cost and efficiency*

In the examples presented here, the CPU time used is typically very small and, hence, the number of evaluations of the constitutive relations that a substepping scheme needs during the integration of a particular problem, can be employed to assess the computational cost of the integration scheme. Given a single strain increment with no substepping, two evaluations of the constitutive relations are needed in the ME substepping scheme whereas six are required in the RKDP substepping scheme. Additionally, each time a step size is rejected, the previous number of evaluations is

repeated and, furthermore, each iteration within the drift correction subroutine can be considered as one more evaluation of the constitutive relations.

Figure 13 shows the computational cost as a function of  $STOL$  (i.e. for  $STOL = 10^{-02}$ ,  $10^{-04}$ ,  $10^{-06}$  and  $10^{-08}$ ) and the strain size for the three types of loading analysed. On the right, the plots correspond to the ME substepping scheme whereas the graphs on the left show the approximations for the RKDP substepping scheme. In general, for large sizes of  $h$  (from 0.01 to 0.1), the larger number of substeps required in the ME substepping scheme to satisfy all values of  $STOL$  typically leads to a largest number of evaluations of the constitutive relationships. Conversely, for small sizes of  $h$  (0.00001), the number of evaluations required is larger in the RKDP substepping scheme. For intermediate sizes of  $h$  (from 0.0001 to 0.001), the best computational efficiency depends on the level of accuracy specified. Thus, for problems in which stringent values of  $STOL$  are specified, the RKDP substepping scheme is probably the most efficient. On the other hand, if looser values of  $STOL$  are tolerable, the ME substepping scheme is possibly the best choice. In the analysis of a practical boundary value problem with finite elements, the size of the strain increments will typically vary widely at each integration point. For this reason, the ME substepping scheme is often used in practice.

## CONCLUSIONS

The dependence on specific volume of the critical state stress-strain relations for saturated soils is central to the accuracy achieved when integrating the model via a numerical method whose order of accuracy is higher than one. This dependence should, therefore, be included in the substepping schemes by using a consistent update of specific volume during the numerical integration.

By noting the fundamental nature of explicit integration, a direct methodology to verify and assess the computational performance of any integration scheme has been developed. All that is required is to plot the error incurred by the numerical scheme against the size of the strain increment (i.e. the known or driven variable of the problem) for various input increment sizes and verify that the rate of convergence is in correspondence with the order of local/global accuracy of the numerical method used. This way of plotting the results is also useful to select the optimal step size for an explicit substepping strategy when error control is to be used.

Additionally, a new form of plotting the computational outcomes for explicit substepping algorithms is proposed and its applicability to check certain computational aspects of these explicit algorithms is successfully demonstrated for different stress paths. More specifically, these new plots represent an ideal platform for assessing the performance of the substepping method, as they do not only provide information on the accuracy achieved by the algorithm but also advise on how the internal substepping tolerance *STOL* influences this accuracy. Consequently, these performance maps may be employed to assess the value of *STOL* that the user must prescribe to reach a particular value of the local error, while also providing information for an estimation of the corresponding computational cost.

Finally, the results show that the substepping methods are capable of controlling the global error so that it satisfies the stress error tolerance *STOL* for all the cases considered.

## APPENDIX

The incremental form of Equation 1 expresses the increments of effective stresses in terms of the increments of strains:

$$\Delta\boldsymbol{\sigma}' = \mathbf{D}\Delta\boldsymbol{\varepsilon} \quad (\text{A1})$$

where  $\mathbf{D}$  is the elastic matrix  $\mathbf{D}_e$  (if no plastic yielding occurs) or the elasto-plastic matrix  $\mathbf{D}_{ep}$  when the given strain increment causes plastic yielding.

In the context of the modified Cam clay model, the symmetric elastic matrix  $\mathbf{D}_e$  and the elasto-plastic matrix  $\mathbf{D}_{ep}$  can be expressed as:

$$\mathbf{D}_e = \begin{pmatrix} K + \frac{4}{3}G & K - \frac{2}{3}G & K - \frac{2}{3}G & 0 & 0 & 0 \\ & K + \frac{4}{3}G & K - \frac{2}{3}G & 0 & 0 & 0 \\ & & K + \frac{4}{3}G & 0 & 0 & 0 \\ \text{symm} & & & G & 0 & 0 \\ & & & & G & 0 \\ & & & & & G \end{pmatrix} \quad (\text{A2})$$

$$\mathbf{D}_{ep} = \mathbf{D}_e \left( \mathbf{I} - \frac{\mathbf{b}\mathbf{a}^T \mathbf{D}_e}{A + \mathbf{a}^T \mathbf{D}_e \mathbf{b}} \right) \quad (\text{A3})$$

where the specific forms of the scalar function  $A$  and the gradient vectors  $\mathbf{a}$  and  $\mathbf{b}$  are, respectively:

$$A = -\frac{vp_0'}{\lambda - \kappa} \frac{\partial f}{\partial p_0'} \frac{\partial g}{\partial p'} \quad (\text{A4})$$

$$\mathbf{a} = \frac{\partial f}{\partial \boldsymbol{\sigma}'} \quad (\text{A5})$$

$$\mathbf{b} = \frac{\partial g}{\partial \boldsymbol{\sigma}'} \quad (\text{A6})$$

where  $f$  is the yield function and  $g$  is the plastic potential.

The incremental form of Equation 2 expresses the increments of the hardening parameter  $H$  during yielding:

$$\Delta H = \Delta \lambda B \quad (\text{A7})$$

where,

$$\Delta \lambda = \frac{\mathbf{a}^T \mathbf{D}_e \Delta \boldsymbol{\varepsilon}}{A + \mathbf{a}^T \mathbf{D}_e \mathbf{b}} = \frac{\mathbf{a}^T \Delta \boldsymbol{\sigma}'_e}{A + \mathbf{a}^T \mathbf{D}_e \mathbf{b}} \quad (\text{A8})$$

$$B = \frac{vp_0'}{\lambda - \kappa} \frac{\partial g}{\partial p'} \quad (\text{A9})$$

The expression of the secant bulk modulus is obtained using the elastic relationship between specific volume and mean effective stress given by the MCC model:

$$dv^e = -\kappa \frac{dp'}{p'} \quad (\text{A10})$$

and integrating it to give:

$$\Delta v^e = -\kappa \ln \frac{p_f'}{p_i'} \quad (\text{A11})$$

where the subscripts  $i$  and  $f$  indicate initial and final respectively. Equation A11 can be expressed, after some manipulation, as:

$$\Delta p' = p_i' \left[ \exp\left(\frac{-\Delta v^e}{\kappa}\right) - 1 \right] \quad (\text{A12})$$

The relationship between the specific volume and volumetric strains is given by:

$$\frac{dv}{v} = -d\varepsilon_v \quad (\text{A13})$$

Integrating Equation A13 over the same increment:

$$\Delta v = v_i \left( \exp(-\Delta\varepsilon_v) - 1 \right) \quad (\text{A14})$$

Equation 5 for the secant bulk modulus is obtained by combining (A13) and (A14).

Similarly to the derivation of Equation 5, it is trivial to derive an analytical expression for stresses for an isotropic elasto-plastic strain compression of a cylindrical soil sample in which  $\Delta\varepsilon_a = \Delta\varepsilon_r$  (where subscripts  $a$  and  $r$  indicate axial and radial directions respectively). In the context of the MCC model, if the initial stress state  $i$  of a cylindrical soil sample lies on the yield surface with zero deviatoric stress, the final mean effective stress,  $p_f'$ , corresponding to an isotropic elastoplastic strain compression of magnitude  $\Delta\varepsilon_v$  will be given by:

$$p_f' = p_i' \exp\left(\frac{v_i (1 - \exp(-\Delta\varepsilon_v))}{\lambda}\right) \quad (\text{A15})$$

## REFERENCES

1. Tamagnini C, Castellanza R, Nova R. Implicit integration of constitutive equations in computational plasticity. *Revue Française de Génie Civil* 2002; **6**(5): 1051-1067.
2. Solowsky WT. 2008. Unsaturated soils: constitutive modelling and explicit stress integration. PhD thesis, University of Durham, UK.
3. Sloan SW, Abbo AJ, Sheng D. Refined explicit integration of elastoplastic models with automatic error control. *Engineering Computations* 2001; **18**(1-2): 121-154.
4. Ortiz M, Simo JC. An analysis of a new class of integration algorithms for elastoplastic constitutive relations. *International Journal for Numerical Methods in Engineering* 1986; **23**: 353-366.
5. Borja RI. Cam-Clay plasticity, Part II: Implicit integration of constitutive equation based on a nonlinear elastic stress predictor. *Computer Methods in Applied Mechanics and Engineering* 1991; **88**: 225-240.
6. Potts DM, Ganendra D. An evaluation of substepping and implicit stress points algorithms. *Computer Methods in Applied Mechanics and Engineering* 1994; **119**: 341-354.
7. Sloan SW. Substepping schemes for the numerical integration of elastoplastic stress-strain relations. *International Journal for Numerical Methods in Engineering* 1987; **24**: 893-911.
8. Sloan SW, Booker JR. Integration of Tresca and Mohr–Coulomb constitutive relations in plane strain elastoplasticity. *International Journal for Numerical Methods in Engineering* 1992; **33**: 163-196.
9. Abbo AJ. 1997. Finite element algorithms for elastoplasticity and consolidation. PhD thesis, University of Newcastle, Australia.
10. Sloan SW, Abbo AJ. Biot consolidation analysis with automatic time stepping and error control Part I: Theory and Implementation. *International Journal for Numerical and Analytical Methods in Geomechanics* 1999a; **23**: 467-492.

11. Sloan SW, Abbo AJ. Biot consolidation analysis with automatic time stepping and error control Part II: Applications. *International Journal for Numerical and Analytical Methods in Geomechanics* 1999b; **23**: 493-529.
12. Zhao J, Sheng D, Rouainia M, Sloan SW. Explicit stress integration of complex soil models. *International Journal for Numerical and Analytical Methods in Geomechanics* 2005; **29**: 1209-1229.
13. Sheng D, Sloan SW, Gens A, Smith DW. Finite element formulation and algorithms for unsaturated soils. Part I: Theory. *International Journal for Numerical and Analytical Methods in Geomechanics* 2003a; **27**: 745-765.
14. Sheng D, Sloan SW, Gens A, Smith DW. Finite element formulation and algorithms for unsaturated soils. Part II: Verification and application. *International Journal for Numerical and Analytical Methods in Geomechanics* 2003b; **27**: 767-790.
15. Sánchez M, Gens A, Guimarães L, Olivella S. A double structure generalized plasticity model for expansive materials. *International Journal for Numerical and Analytical Methods in Geomechanics* 2005; **29**: 751-787.
16. Pedroso DM, Sheng D, Sloan, SW. Stress update algorithm for elastoplastic models with nonconvex yield surfaces. *International Journal for Numerical Methods in Engineering* 2008; **76**: 2029-2062.
17. Solowski WT, Gallipoli D. Explicit stress integration with error control for the Barcelona Basic Model. Part I: Algorithms formulations. *Computers and Geotechnics* 2010a; **37**(1-2): 59-67.
18. Solowski WT, Gallipoli D. Explicit stress integration with error control for the Barcelona Basic Model. Part II: Algorithms efficiency and accuracy. *Computers and Geotechnics* 2010b; **37**(1-2): 68-81.
19. González NA, Gens A. 2011. Evaluation of a constitutive model for unsaturated soils: stress variables and numerical implementation. Fifth International Conference on Unsaturated Soils Barcelona (eds Alonso E, Gens A), Taylor & Francis Group, 2: 829-835.
20. Cattaneo F, Vecchia GDella, Jommi C. Evaluation of numerical stress-point algorithms on elastic-plastic models for unsaturated soils with hardening dependent on the degree of saturation. *Computers and Geotechnics* 2014; **55**: 404-415.

21. Roscoe KH, Burland JB. 1968. On the generalised stress-strain behavior of wet clay. *Engineering Plasticity* (eds Heyman J & Leckie FA), Cambridge University Press, Cambridge: 535-609.
22. Zytynski M, Randolph MF, Nova R, Wroth CP. On modelling the unloading-reloading behaviour of soils. *International Journal for Numerical and Analytical Methods in Geomechanics* 1978; **2**: 87-94.
23. Wheeler SJ. 2014. Personal communication.
24. Sheng D, Sloan SW, Yu HS. Aspects of finite element implementation of critical state models. *Computational mechanics* 2000; **26**: 185-196.
25. Potts DM, Gens A. A critical assessment of methods of correcting for drift from the yield surface in elasto-plastic finite element analysis. *International Journal for Numerical Methods in Engineering* 1985; **9**: 149-159.
26. Shampine LF. 1994. *Numerical Solution of Ordinary Differential Equations*. Chapman & Hall, London.

Table 1. Soil parameter values and initial state used in the simulations

$\lambda = 0.12$	$\nu = 0.3$	$p'_0 = p'_A = 50 \text{ kPa}$
$\kappa = 0.05$	$M = 1.2$	$N = 2.0$

Table 2. Relative error on effective stress for a single elasto-plastic isotropic loading step (single step explicit integration schemes with update of specific volume only at the end of the integration increment)

$\Delta\varepsilon_v$	FE1	ME2	RKDP4	RKDP5
$1 \cdot 10^{-6}$	$7.50 \cdot 10^{-11}$	$6.38 \cdot 10^{-12}$	$6.38 \cdot 10^{-12}$	$6.38 \cdot 10^{-12}$
$1 \cdot 10^{-5}$	$7.50 \cdot 10^{-9}$	$6.37 \cdot 10^{-10}$	$6.38 \cdot 10^{-10}$	$6.38 \cdot 10^{-10}$
$1 \cdot 10^{-4}$	$7.49 \cdot 10^{-7}$	$6.34 \cdot 10^{-8}$	$6.38 \cdot 10^{-8}$	$6.38 \cdot 10^{-8}$
$1 \cdot 10^{-3}$	$7.43 \cdot 10^{-5}$	$6.03 \cdot 10^{-6}$	$6.38 \cdot 10^{-6}$	$6.38 \cdot 10^{-6}$
$1 \cdot 10^{-2}$	$6.84 \cdot 10^{-3}$	$3.21 \cdot 10^{-4}$	$6.36 \cdot 10^{-4}$	$6.36 \cdot 10^{-4}$
$1 \cdot 10^{-1}$	$3.24 \cdot 10^{-1}$	$8.24 \cdot 10^{-2}$	$6.31 \cdot 10^{-2}$	$6.31 \cdot 10^{-2}$

Table 3. Relative error on effective stress for a single elasto-plastic isotropic loading step (single step explicit integration schemes with consistent update of  $\nu$ )

$\Delta\varepsilon_v$	ME2	RKDP4	RKDP5
$1 \cdot 10^{-6}$	$4.26 \cdot 10^{-16}$	--	--
$1 \cdot 10^{-5}$	$3.46 \cdot 10^{-13}$	--	--
$1 \cdot 10^{-4}$	$3.48 \cdot 10^{-10}$	--	--
$1 \cdot 10^{-3}$	$3.44 \cdot 10^{-7}$	$2.34 \cdot 10^{-13}$	$5.61 \cdot 10^{-16}$
$1 \cdot 10^{-2}$	$3.12 \cdot 10^{-4}$	$1.87 \cdot 10^{-8}$	$6.35 \cdot 10^{-10}$
$1 \cdot 10^{-1}$	$1.25 \cdot 10^{-1}$	$1.53 \cdot 10^{-4}$	$3.94 \cdot 10^{-4}$

Table 4. Relative error on effective stress for a single elasto-plastic isotropic loading step (substepping integration schemes with update of specific volume only at the end of the integration increment,  $\Delta\varepsilon_v = 0.1$ )

<i>STOL</i>	ME with substepping	TS	TF	RKDP with substepping	TS	TF
$1 \cdot 10^{-4}$	$5.77 \cdot 10^{-4}$	95	2	$6.31 \cdot 10^{-2}$	1	0
$1 \cdot 10^{-6}$	$6.05 \cdot 10^{-5}$	950	3	$1.19 \cdot 10^{-2}$	5	3
$1 \cdot 10^{-8}$	$6.07 \cdot 10^{-6}$	9505	5	$4.64 \cdot 10^{-3}$	13	2

Table 5. Relative error on effective stress for a single elasto-plastic isotropic loading step (substepping integration schemes with consistent update of specific volume during the substepping,  $\Delta\varepsilon_v = 0.1$ )

<i>STOL</i>	ME with substepping	TS	TF	RKDP with substepping	TS	TF
$1 \cdot 10^{-04}$	$3.58 \cdot 10^{-05}$	91	2	$4.46 \cdot 10^{-05}$	2	2
$1 \cdot 10^{-06}$	$3.58 \cdot 10^{-07}$	910	3	$1.99 \cdot 10^{-07}$	5	2
$1 \cdot 10^{-08}$	$3.58 \cdot 10^{-09}$	9105	4	$1.71 \cdot 10^{-09}$	13	2

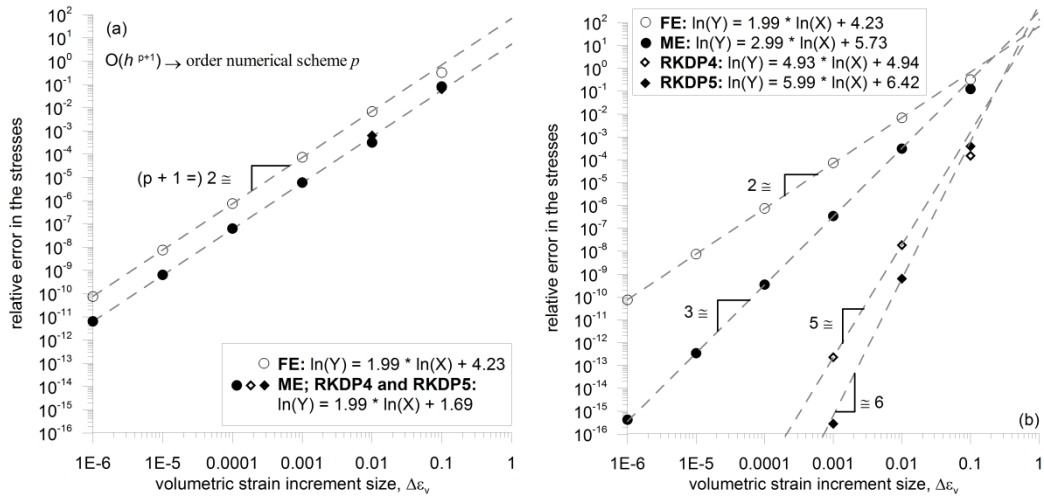


Figure 1. Relative error in stresses for single step explicit integration schemes against strain increment size for a single elasto-plastic isotropic loading increment: (a) with update of specific volume only at the end of the integration increment; (b) with consistent update of specific volume during the integration increment.

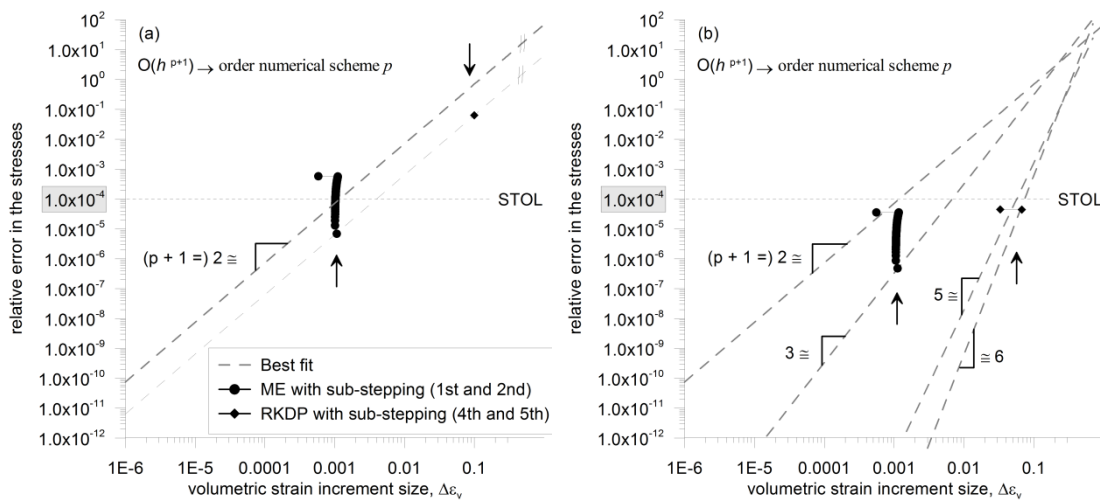


Figure 2. Relative error in stresses for substepping integration schemes with  $STOL = 10^{-4}$  against strain increment size for a single elasto-plastic isotropic loading increment: (a) update of specific volume only at the end of the integration increment; (b) with consistent update of specific volume during the integration increment.

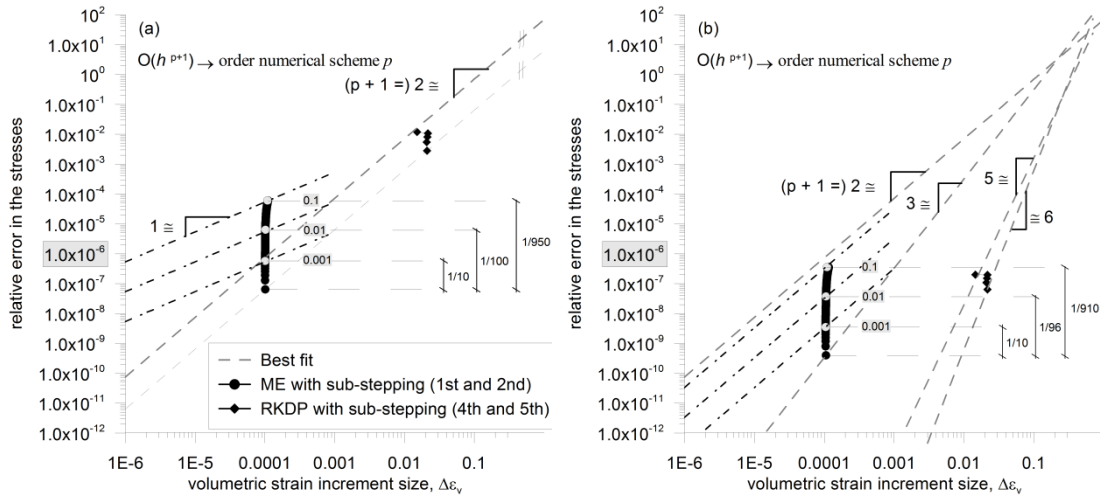


Figure 3. Relative error in stresses for substepping integration schemes with  $STOL = 10^{-6}$  against strain increment size for a single elasto-plastic isotropic loading increment: (a) update of specific volume only at the end of the integration increment; (b) with consistent update of specific volume during the integration increment.

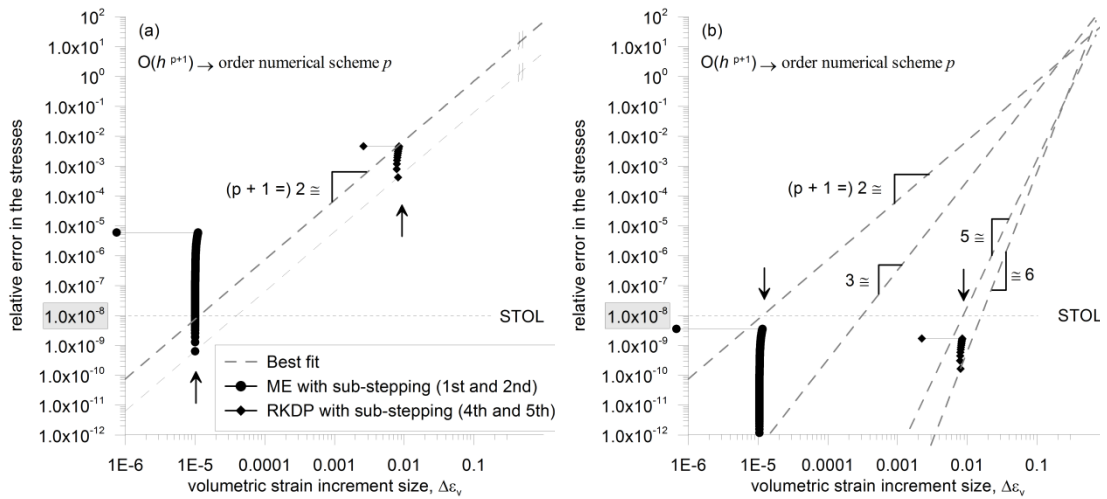


Figure 4. Relative error in stresses for substepping integration schemes with  $STOL = 10^{-8}$  against strain increment size for a single elasto-plastic isotropic loading increment: (a) update of specific volume only at the end of the integration increment; (b) with consistent update of specific volume during the integration increment.

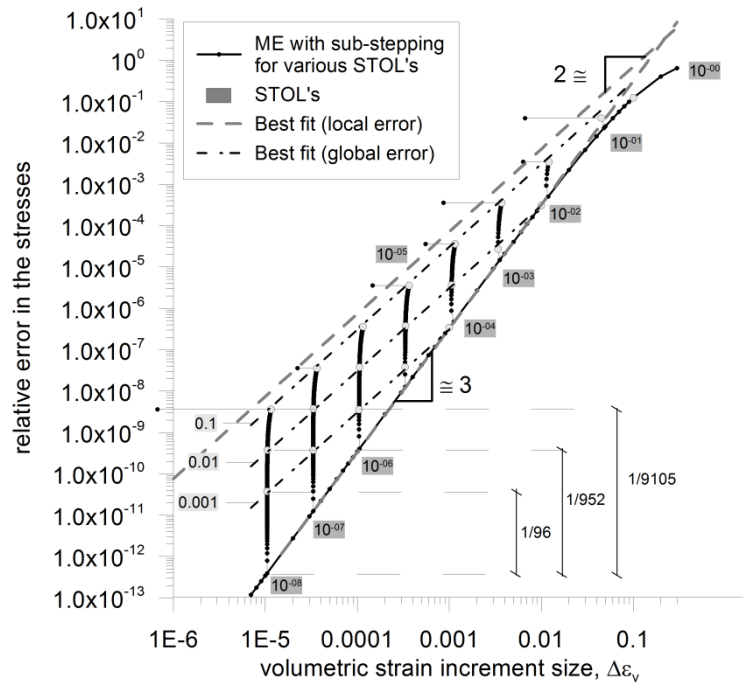


Figure 5. Relative error behaviour in stresses for ME with substepping integration scheme with different *STOL* values against strain increment size for a single elasto-plastic isotropic loading increment.

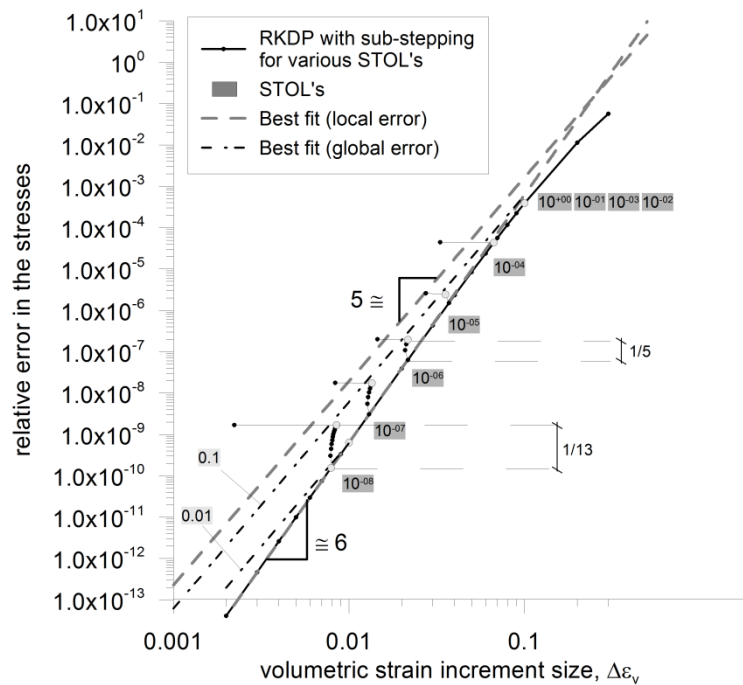


Figure 6. Relative error behaviour in stresses for RKDP substepping scheme with different *STOL* values against strain increment size for a single elasto-plastic isotropic loading increment.

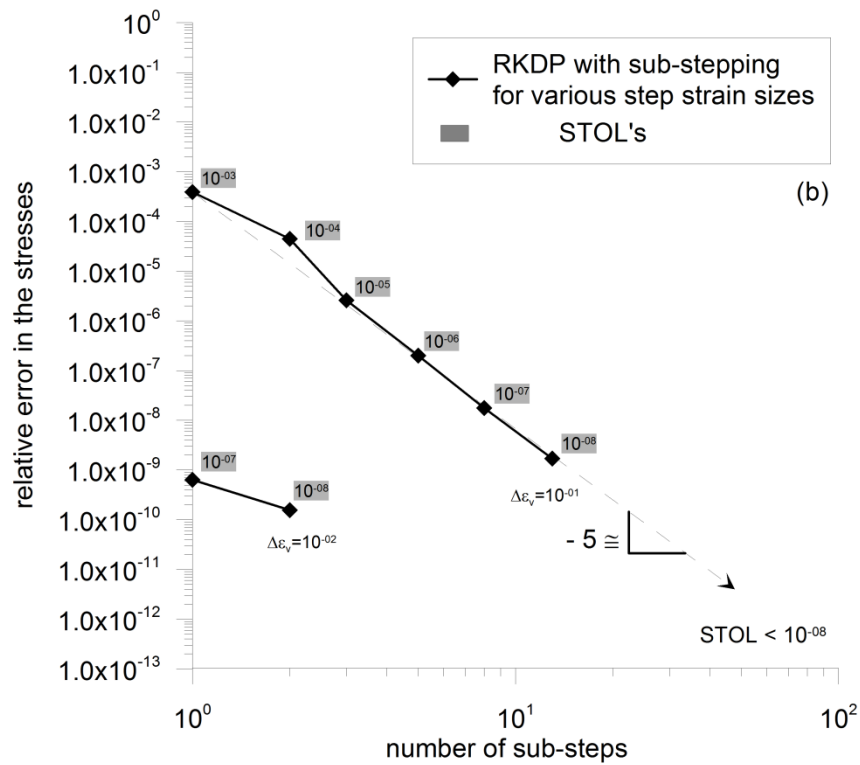
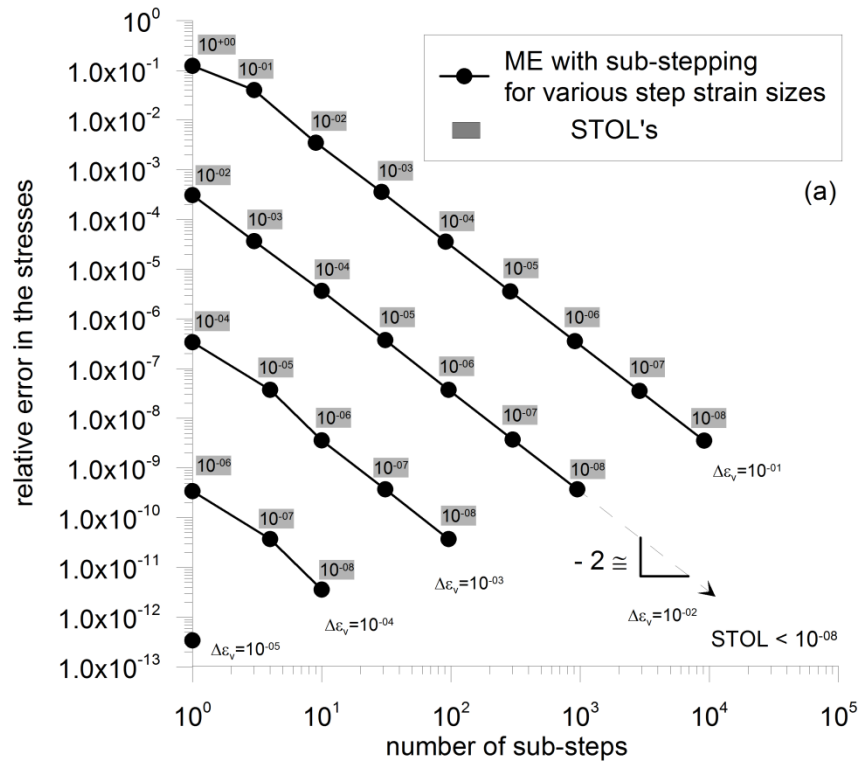


Figure 7. Relative error behaviour against number of substeps for a single elasto-plastic isotropic loading increment: (a) ME substepping scheme; (b) RK substepping scheme.

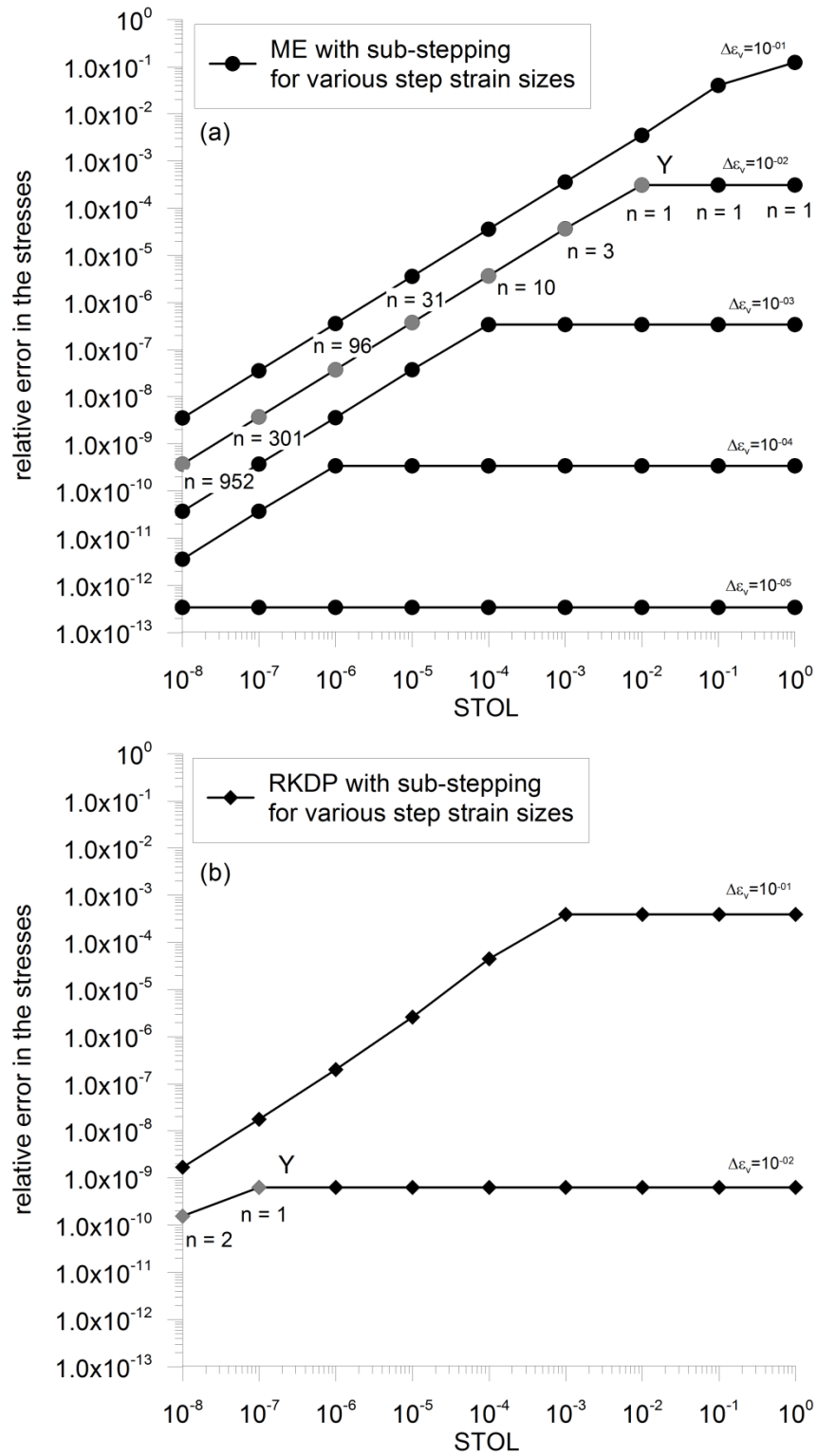


Figure 8. Relative error behaviour against  $STOL$  for a single elasto-plastic isotropic loading increment: (a) ME substepping scheme; (b) RK substepping scheme.

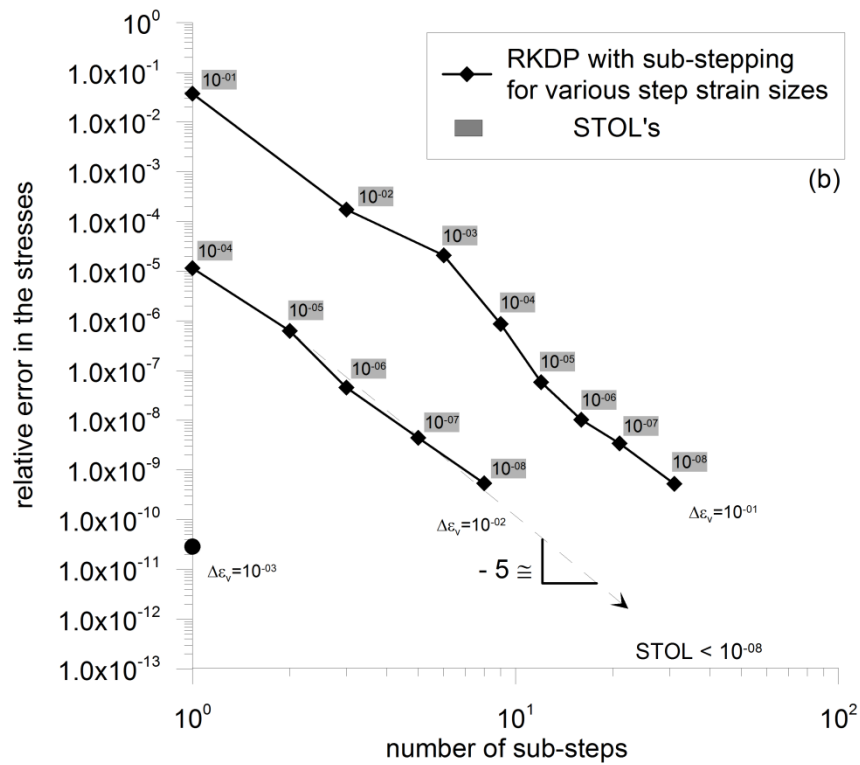
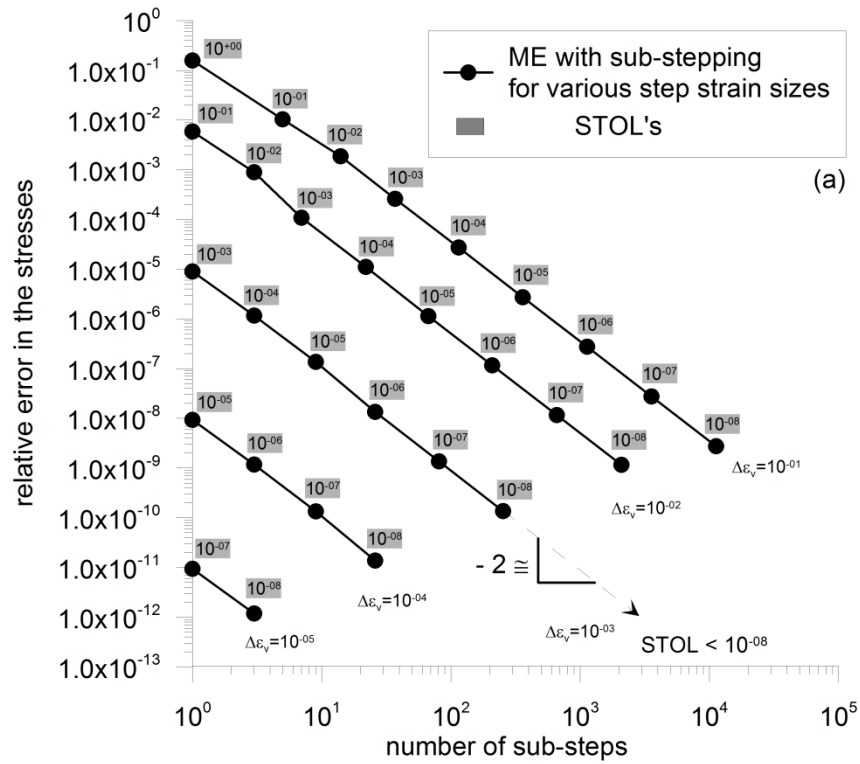


Figure 9. Relative error behaviour against number of substeps for a single elasto-plastic axial loading increment with zero radial strains (a) ME substepping scheme; (b) RK substepping scheme.

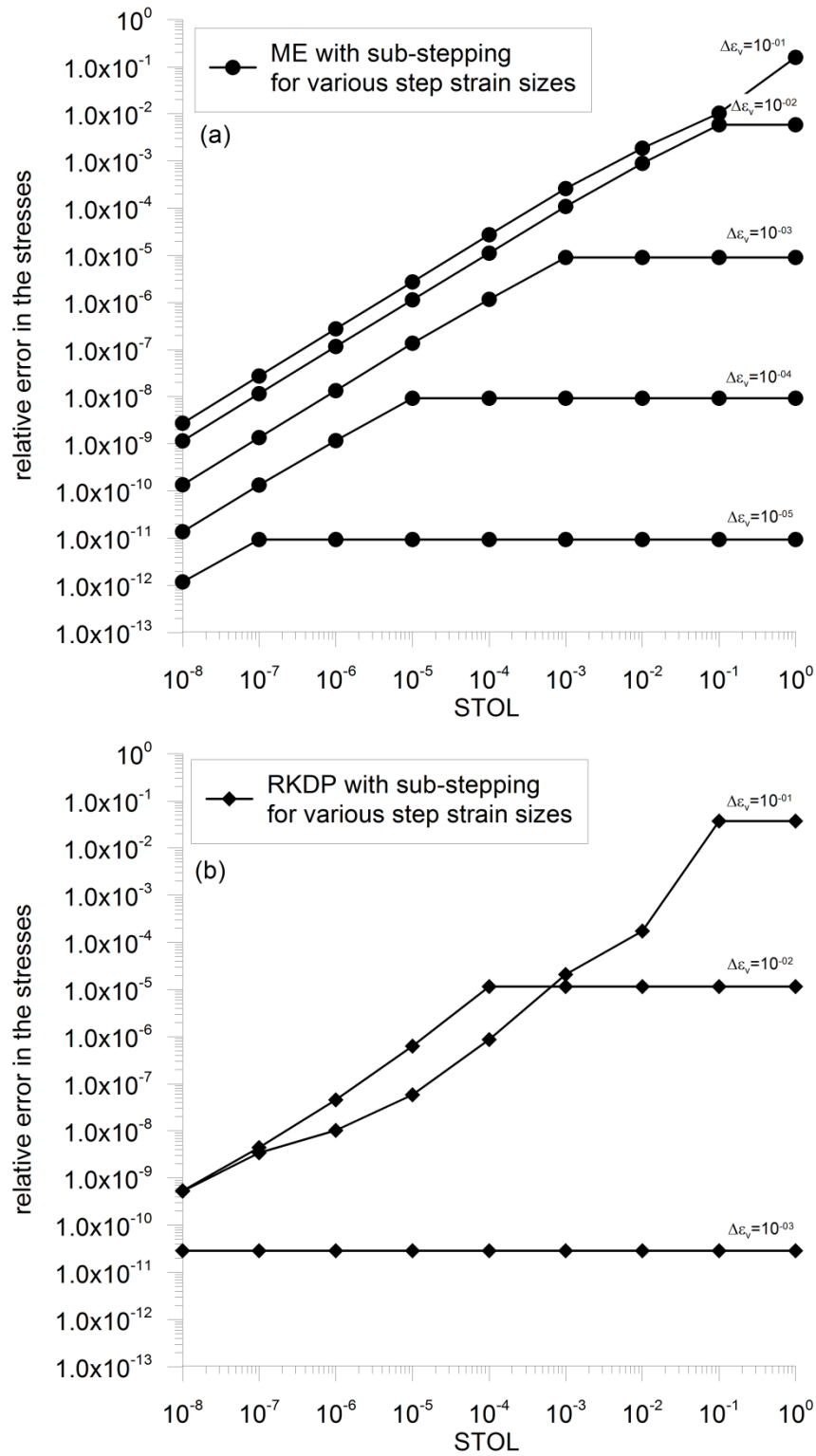


Figure 10. Relative error behaviour against  $STOL$  for a single elasto-plastic axial loading increment with zero radial strains (a) ME substepping scheme; (b) RK substepping scheme.

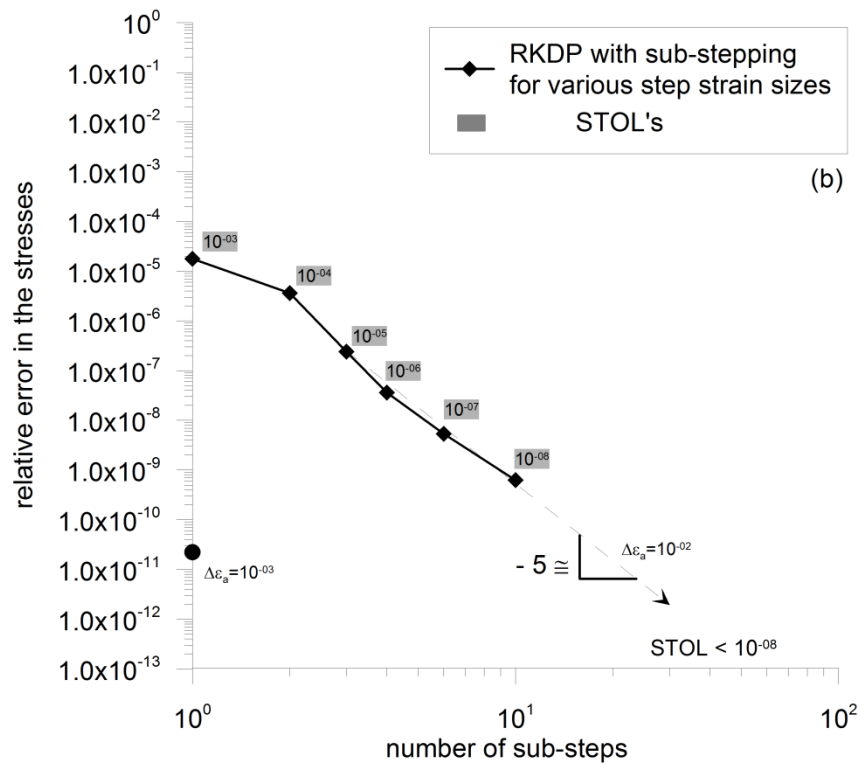
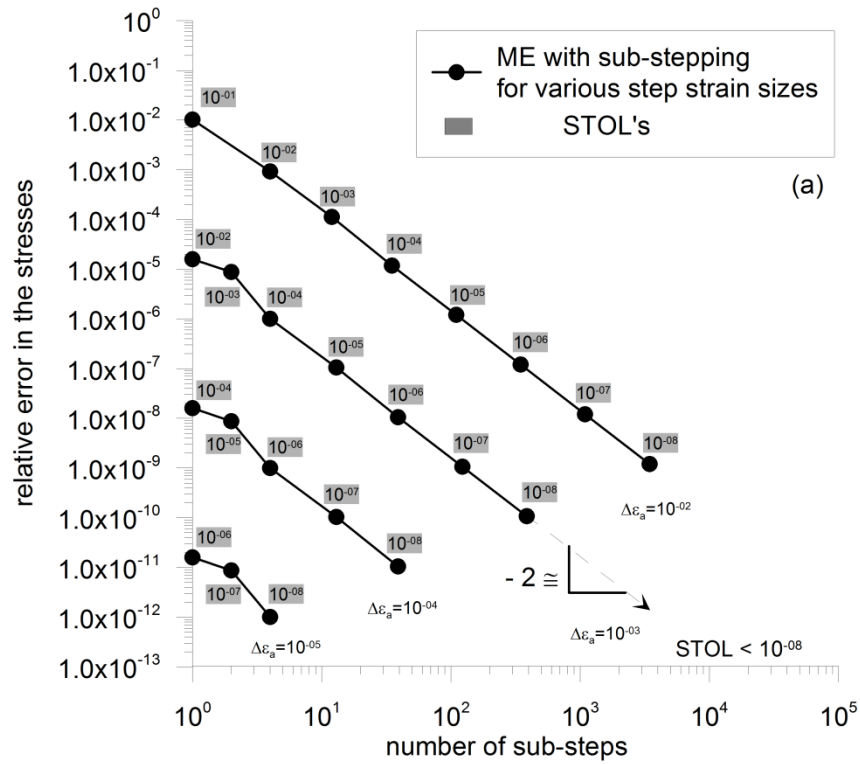


Figure 11. Relative error behaviour against number of substeps for a single elasto-plastic undrained shear loading increment: (a) ME substepping scheme; (b) RKDP substepping scheme.

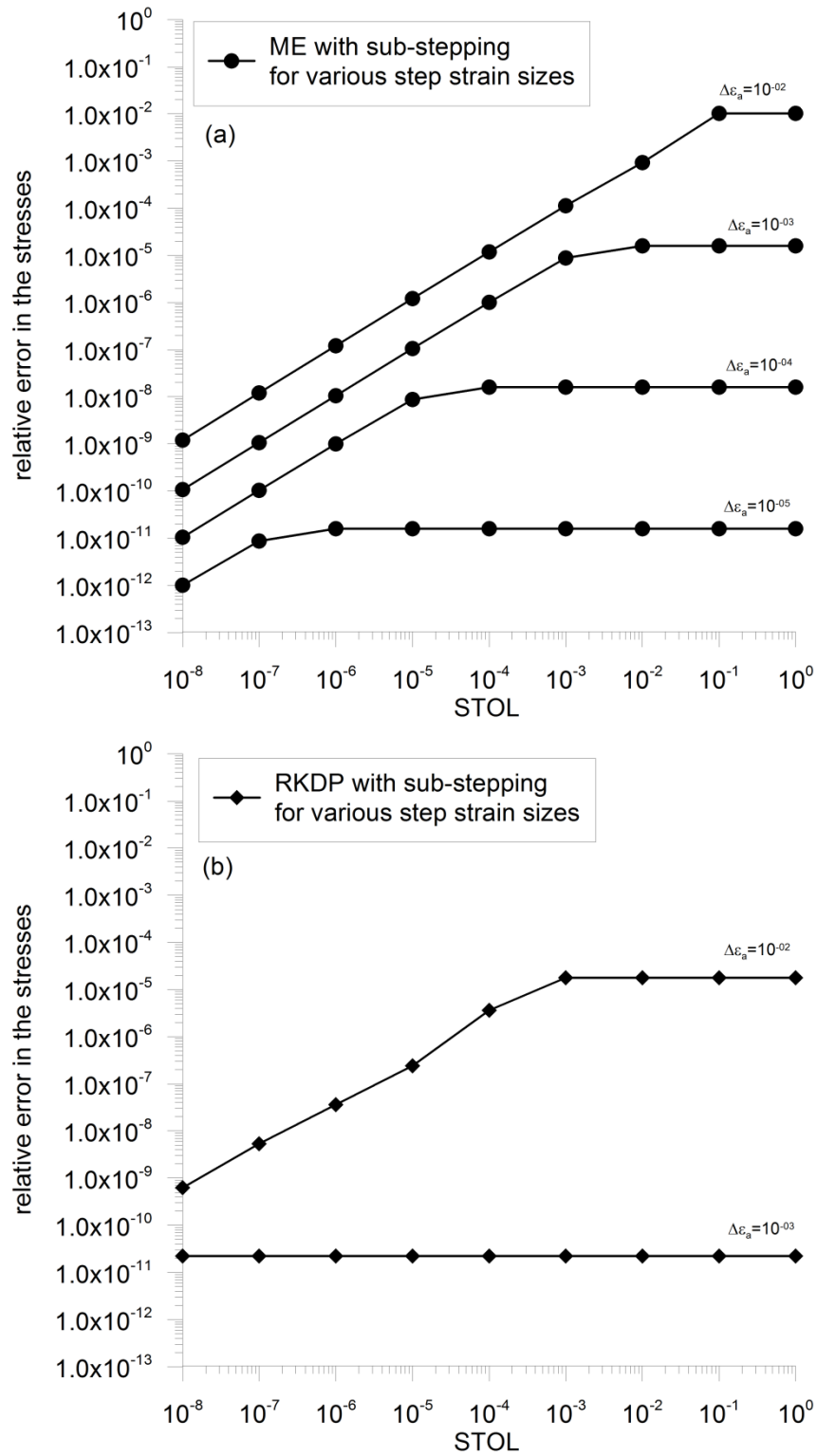


Figure 12. Relative error behaviour against  $STOL$  for a single elasto-plastic undrained shear loading increment: (a) ME substepping scheme; (b) RKDP substepping scheme.

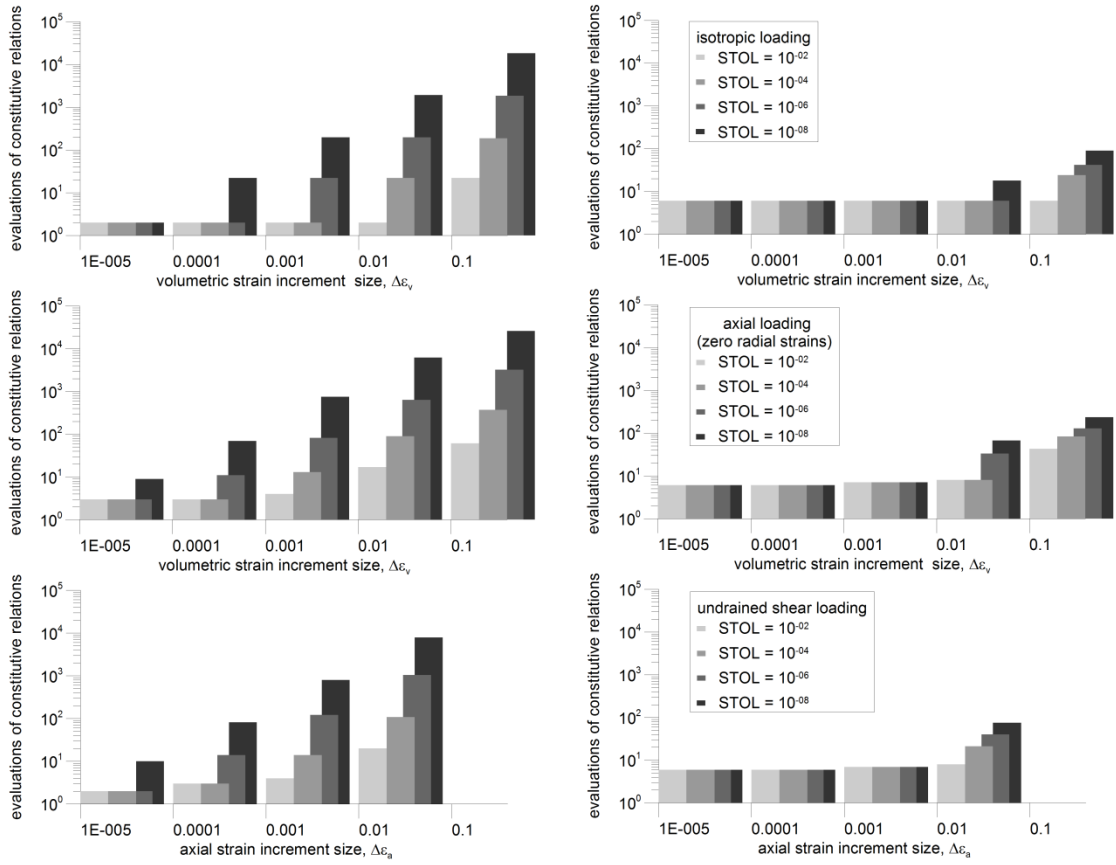


Figure 13. Computational cost for different *STOL* values against strain increment size: (right) ME substepping scheme; (left) RK substepping scheme.